Journal of
Applied and Computational Mechanics

Shahid Chamran
University of Ahvaz

Research Paper

2D Planar Simulation of Collisions between Liquid Droplets and Solid Particles in a Gas

Dmitrii V. Antonov[1], Roman M. Fedorenko[2], Pavel A. Strizhak[3]

[1] National Research Tomsk Polytechnic University, 30, Lenin Avenue, Tomsk, 634050, Russia, Email: antonovdv132@gmail.com

[2] National Research Tomsk Polytechnic University, 30, Lenin Avenue, Tomsk, 634050, Russia, Email: vfedrm@gmail.com

[3] National Research Tomsk Polytechnic University, 30, Lenin Avenue, Tomsk, 634050, Russia, Email: pavelspa@tpu.ru

Abstract. Here we present a 2D planar simulation of the collisions between liquid droplets and solid particles that are most often used in industrial applications. The collisions are modeled using a combination of Volume of Fluid and Level Set methods. We study the impact of the particle-to-droplet size ratio and the shape of solid particles on the collision behavior and interaction regimes. The findings are presented in the form of collision regime maps. The interaction regimes are also distinguished for binary droplet collisions: deposition, separation, and disintegration. We show the impact of density, viscosity, and surface tension on the droplet collision regime maps as well as on the number of secondary fragments. The practical value of the research comes from the newly established differences of collision regimes between droplets and particles of different shapes and sizes.

Keywords: Droplet and particle collisions; interaction regimes; Volume of Fluid Method; Level Set Method; different shapes; 2D planar simulation.

1. Introduction

Droplet interactions with solid particles and surfaces remain an important subject of research [1–4]. They are involved in many technological applications [5–9]: spray coating and cooling, fuel injection into internal combustion engines, firefighting, inkjet printing, film formation, nanofluids etc. It is important to explore these processes because they lead to the redistribution of droplet sizes and velocities in an aerosol flow. Unlike droplet interactions with solid flat surfaces, droplets colliding with round surfaces remain understudied. The best known studies in this field are theoretical [10–12]. Volume of Fluid (VOF) [1, 10], lattice Boltzmann method (LBM) [13, 14], Level Set [15–17] and Front Tracking [18–20] are the main approaches to modeling droplet collisions with solid particles. At this point, we can single out just a few experimental studies (for instance, [21–24]) on droplet-particle collision behavior in a gas.

Malgarinos et al. [1] presented their numerical study of collisions between liquid droplets and a stationary spherical particle with the Weber number ranging from 8 to 80. They also explored the impact of droplet-to-particle size ratio in the range of 0.31 to 1.24 on the position of the boundaries between the droplet-particle interaction regimes. The authors distinguished the following interaction regimes: bounce and disintegration into secondary droplets.

Yoon and Shin [10] studied collisions of water, isopropyl alcohol, and acetone droplets with solid particles experimentally and theoretically. They also explored the impact of the surface temperature on the collision outcomes. The results of numerical modeling for droplet-particle collisions were presented by Gac and Gradoń [13], who also investigated how the shape of solid particles (spherical, elliptical, and cubic) affected the interaction regimes. They established three outcomes of collisions between droplets and solid particles: deposition, ripping and coating, and skirt scattering. The outcomes are primarily caused by the Weber numbers reaching certain critical values. But Ref. [13] did not address the role of the properties of liquids interacting in the droplet-particle system. Efforts were made to estimate the impact of liquid viscosity and density on droplet collision behavior [23]. However, the estimates of collision regimes are largely qualitative, comparing the experimental and theoretical data without generalizing the results in the form of $B(We)$ regime maps.

Pawar et al. [25] presented their experimental research into droplet-particle collisions at relatively low capillary numbers. They distinguished the following collision outcomes: agglomeration (merging), where a droplet would stick to the surface of the particle, and stretching separation (breaking), where the droplet would interact with the particle to form secondary fragments. The boundary between agglomeration and stretching separation was determined as an approximation, inversely proportional to the Weber number. Secondary fragments were found to form at the impact parameter $B=2b/(D_s+D_L)$ ranging from 0.4 to 0.8, and the largest number of satellite droplets were observed at $B=0.5$.

Yan-Peng and Huan-Ran numerically studied droplet-particle collisions in wide ranges of particle sizes (from 1.26 cm to 50 cm) and impact velocities (fro,m 0.2 m/s to 0.85 m/s). However, their research was limited to the cases where the droplet-particle

size ratio did not exceed 1. Charalampous and Hardalupas [22] researched the interaction between small droplets and relatively large particles and reported on the conditions for the crown formation. The main assumption in Refs. [1, 3, 13, 23, 25] was zero motion of particles. The limitations of this approach to the analysis of binary collisions have been extensively discussed [21, 26–28]. In the present research, we study the collisions between moving droplets and stationary particles. The relative motion of the droplet and the particle is taken into account (with the so-called resultant velocity). A numerical simulation model was then developed and verified against the available experiments. All studies in the field of droplet-particle interactions in terms of their kinetics and geometry are generally classified into five groups [29]: droplet impact onto planar surfaces [30–35], droplet collision with the cross section of a cylindrical object [36–38], droplet impact with lateral surface of a cylinder [39–42], droplet impact onto a stationary solid sphere [13, 43–48], and droplet-particle collision in air [24, 49].

Interesting experimental findings on the interactions between a single droplet, 2.48–2.61 mm in diameter (cold and heated), and a stationary hydrophobic particle, 3 mm in diameter, were reported by Mitra et al. [50]. The experiments were carried out at low Weber numbers (0.9–47.1) using high-speed visualization. Changes in the particle temperature were observed in different collision outcomes. In the presence of heat transfer at the particle/droplet interface, nucleate boiling was found to prevent the occurrence of the regime where the film thickness decreases significantly over time until it reaches the size of the boundary layer. Mitra et al. [51] investigated the interaction of small particles (1.13±0.02 mm in diameter) with larger sessile droplets (3.41±0.01 mm in diameter) using high-speed video recording with varying impact velocity (Weber number ranging from 0.2 to 13.5). They proposed a one-dimensional approach to analyzing the impact of six major forces—gravity, capillary force, fluid drag, buoyancy, pressure, and added mass—on droplet-particle collisions. A 3D model was developed using the volume of fluid method and the dynamic meshing technique. The 3D model was in good agreement with experimental observations of the overall collision dynamics including droplet deformation.

Yoon and Shin [52] numerically investigated the spreading processes following droplet collisions with a stationary spherical particle in the Weber number range of 30 to 90 and Ohnesorge number range of 0.0013 to 0.7869. They established the impact of liquid viscosity and surface curvature on the maximum spreading of the droplet on the particle surface. The numerical simulation showed acceptable agreement with the existing experimental data: the deviations did not exceed 15%.

Wu and Chen [53] reported on the results of direct numerical simulation of collisions between a droplet and a particle, both moving under gravity, using the lattice Boltzmann method. They studied the impact of Bond number, particle surface wettability, particle-to-droplet size ratio, and non-sphericity factor on droplet-particle collision behavior. The conditions of the bounce regime occurrence were established, which, according to Wu and Chen [53], can explain the collision mechanism between moving droplets and particles. Pasternak et al. [54] described their research findings on collisions between large, solid, moving droplets and smaller droplets using high-speed measurements. Collision regime maps were constructed in the $B(We)$ coordinates. Rebound, deposition and separation, or splashing were distinguished as the collision regimes.

The practical value of the present research comes from the newly established differences of collision regimes between droplets and particles of different shapes and sizes. These aspects have not yet been established experimentally [25] or using advanced models of droplet-particle collisions [1–4, 10, 11, 14]. With a switch from spherical droplets to cubic or octahedral ones, the regime boundaries change drastically on the maps and so does the number of secondary fragments formed after droplet-particle interactions. The more facets a solid particle has, the higher the probability of disintegration, which contributes to the breakup of the thin liquid film flowing over the particle. It is possible to manage the droplet-particle interaction regimes not only by varying the particle shape but also by controlling the thermophysical and rheological properties of the particle and the droplet (density, viscosity, and surface tension) before the interaction. That would require a comparative analysis of the regime maps and characteristics of secondary fragments (their size and number) during the interaction between droplets and particles of various shapes and with different thermophysical and rheological properties.

The aim of this research was to determine the transition boundaries between the droplet-particle interaction regimes based on the 2D planar simulations of collisions between water droplets and solid particles. The originality of the research consists in studying the non-conventional droplet-particle collision outcomes (deposition, separation, and disintegration), which are important for the development of various practical applications, in particular, for thermal power stations and other industrial units powered by multi-component composite fuels. We have studied the impact of liquid viscosity, density, and surface tension, as well as the particle shape and droplet-particle size ratio on the non-conventional droplet-particle collision regimes (deposition, separation, and disintegration) and the number and size of secondary fragments. We used a coupled Volume of Fluid and Level Set method accounting for possible simplifications (in particular, fewer levels of mesh refinement, the choice of the optimal initial mesh size and time increment, etc.). Here we aimed at reducing the computation time while maintaining the reasonable qualitative agreement with our own experimental data. The chosen ranges of physical properties (density range of 500 to 2000 kg/m³, surface tension range of 0.007 to 0.7 N/m and viscosity range of 0.0001 to 0.01 Pa.s) reflect the corresponding properties of water-based slurries, solutions, and emulsions in a wide variety of applications: firefighting, fuel systems, thermal and flame liquid treatment, spray irrigation systems, surface treatment and painting, etc.

2. Numerical Simulation in 2D Planar Concept

2.1 Droplet collision mechanism

Collisions between 2D liquid droplets and cylindrical solid particles are commonly described accounting for the physical properties: density, viscosity, surface tension, etc. We used three dimensionless criteria: Weber number $\mathrm{We} = \rho U_{rel}^2 D_0 / \sigma$; Reynolds number $\mathrm{Re} = \rho U_{rel} D_0 / \mu$; diameter ratio $\Delta = D_L / D_S$.

Three collision regimes were distinguished for modeling: deposition, separation, and disintegration. The collisions between 2D liquid droplets and cylindrical particles were modeled accounting for their relative motion. Fig. 1 shows the general scheme of collisions between water droplets and solid particles, while Fig. 2 schematically shows the collisions of water droplets with different-shaped particles: sphere, cube, and octahedron. In this research, we used a 2D droplet-particle collision model to obtain a reasonable agreement between the modeling and experimental results at minimum computational cost compared to 3D modeling [55, 56]. Quantitatively, the results of the calculations illustrate a need to address 3D effects to analyze droplet-particle collisions, which we are going to consider in our future research in this field. Table 1 presents the physical properties of the droplets, particles, and air.

Table 1. Physical properties of droplets, particle and air [57].

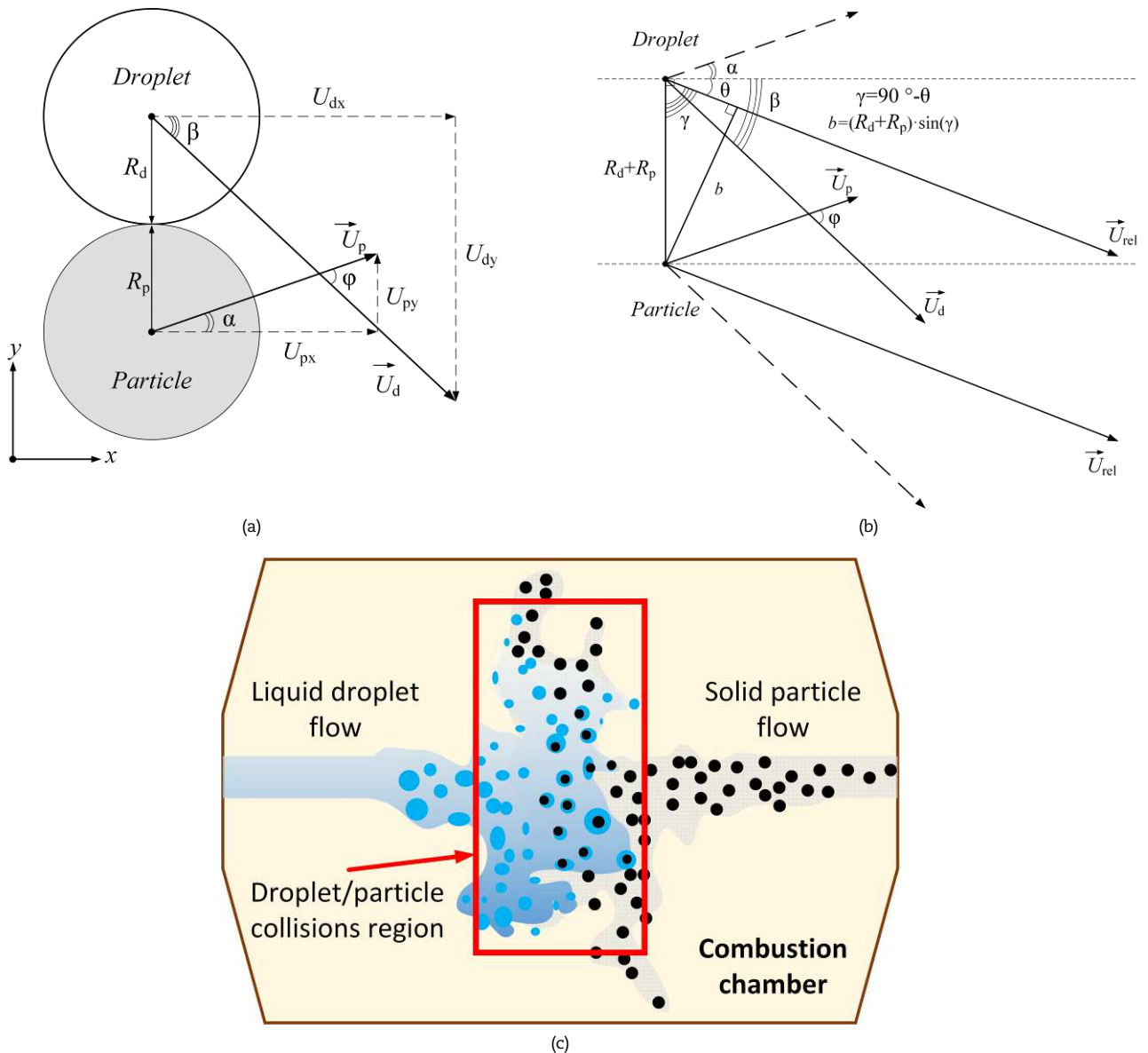| Material	Physical properties
Water-liquid	$\rho = 1000$ kg/m³; $\sigma = 0.073$ N/m; $\mu = 0.001004$ kg/(m·s)
Coal particle	$\rho = 1340$ kg/m³
Air	$\rho = 1.225$ kg/m³; $\mu = 1.7894 \cdot 10^{-5}$ kg/(m·s)

(a)

(b)

(c)

Fig. 1. Scheme of a droplet-particle collision: (a) – visual representation of the collision moment; (b) – vector diagram for calculating the linear parameter b; (c) – implementation in practical applications (for example, steam boilers).

Below are the notes on the characterization of the parameter b in the form of equations. Note that Eqs. (1)-(6) are very complex and can be applied to cases of mobile coal particles. In the case of zero particle velocity ($U_p = 0$) can be simplified. The assumption ($U_p = 0$) was taken into account in this paper.

$$b = \left| \left(R_d + R_p \right) \cdot \sin(\gamma) \right|; \tag{1}$$

$$\gamma = 90° - \theta; \tag{2}$$

$$\theta = \arcsin \left(U_p \cdot \sin \left(180° - (\alpha + \beta) \right) / U_{rel} \right) - \alpha; \tag{3}$$

$$U_d = \sqrt{U_{dx}^2 + U_{dy}^2}, \ U_p = \sqrt{U_{px}^2 + U_{py}^2}; \tag{4}$$

$$\alpha = \operatorname{arctg} \left[\frac{U_{dy}}{U_{dx}} \right], \ \beta = \operatorname{arctg} \left[\frac{U_{py}}{U_{px}} \right]; \tag{5}$$

$$U_{rel} = \sqrt{U_d^2 + U_p^2 - 2 \cdot U_d \cdot U_p \cdot \cos(\alpha + \beta)}. \tag{6}$$

The linear parameter B is traditionally used for studying droplet-droplet and droplet-particle collision regime maps [11, 58, 59]. The linear parameter was given by:
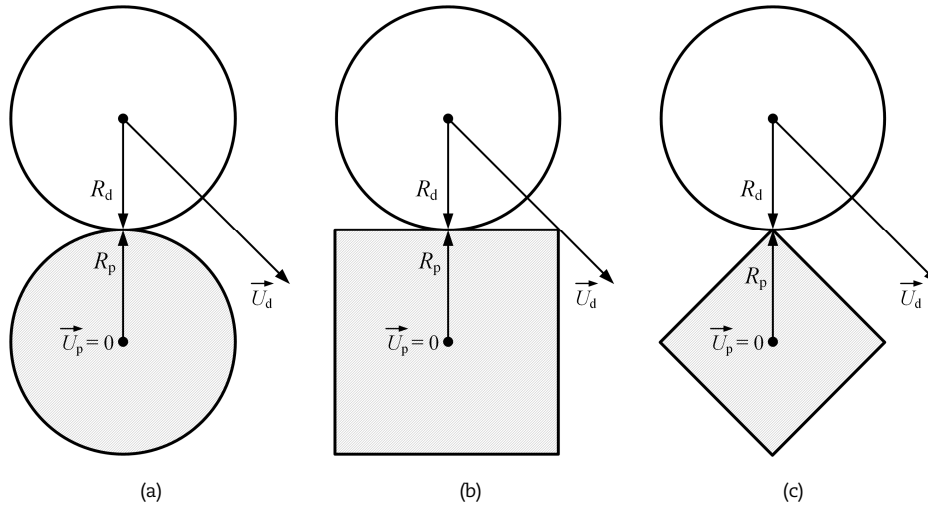
$$B = \frac{2 \cdot b}{D_S + D_L}. \tag{7}$$

Fig. 2. Scheme of a collision between a droplet and a particle with varying shape of the latter: (a) – sphere; (b) – cube; (c) – octahedron.

Note that the heat transfer behavior was not factored in when solving a droplet-particle collision hydrodynamics problem because the difference between the temperatures of the droplets, particles, and surrounding gas was no more than 5 K. In our case, the actual experiments and modeling were performed at room temperature and atmospheric pressure. Solving the heat transfer problem would significantly complicate the system of equations and, hence, add to the computational burden. The heat transfer behavior during interactions is accounted for in [55, 60, 61]. In particular, Gumulya et al. [55] developed a CLSVOF-based three-dimensional numerical model to study the hydrodynamics of water droplets of different diameters colliding with a heated solid particle. The particle temperature was set above the Leidenfrost point of the liquid to study the impact of several key parameters on the film boiling dynamics of the droplet. Mitra et al. [60] investigated the interactions between droplets and particles with a size ratio below unity in the film boiling regime on a spherical particle with high thermal conductivity. In [61], Mitra et al. [60] studied the collision behavior of water droplets (2.9±0.1 mm in diameter) and a stationary brass particle (10 mm in diameter) in the Weber number (We) range from 4 to 104 with and without heat transfer using high speed imaging and computational fluid dynamics (CFD). They identified the conditions under which thermal effects may be paramount. These conditions were accounted for in the numerical studies as part of this work.

2.2 Numerical method

In this work, the numerical model of droplet-particle collisions was based on a CLS-VOF method (hybrid of Level Set and VOF method), just as in Refs. [1, 62], which studied the interactions between solid and liquid phases. It considers the solution of full Navier-Stokes equations to ensure the conservation of mass and momentum in conjunction with the advection of the scalar value known as the fractional volume of fluid $F(x, y, z, t)$. The gaseous and liquid phases are considered to be a single multi-component medium. The solid phase is independent of the liquid and gas phases. The solid phase is only assigned the boundary conditions, and the most important task was to obtain the contact angles determining the outcome of droplet-particle collisions. The volume fraction $F(x, y, z, t)$ is defined as the percentage of volume occupied by the liquid phase in a computational cell with respect to the total volume of the cell. The volume fraction of a phase in a computational cell is taken as $F(x, y, z, t) = 0$ if the cell is empty, $F(x, y, z, t) = 1$ if the cell is occupied by fluid, and $0 < F(x, y, z, t) < 1$ if the interface between the two fluids crosses the cell. In each control volume, the volume fractions of all phases sum to unity:

$$\sum_{i=1}^{2} F_i = 1. \tag{8}$$

To account for the specific aspects of droplet-particle interactions, one more source in the form of $\vec{f}_{WFM}$ [1, 62], known as Adhesion Stress term (volumetric), is added to the hybrid of Level Set and VOF method interpretation [63]. For more details on the calculation of $\vec{f}_{WFM}$, see Ref. [62]. Note that we only considered the cases of dynamic contact angle for cylindrical particles using the corresponding user-defined functions introduced into Ansys Fluent following the recommendations by Malgarinos et al. [62]. Note that in all simulations we used a constant contact angle of 90°. But effects of different contact angle were additionally estimated in Supplementary materials A-C. It is important to consider the variations in the contact angle for different-shaped particles for a more detailed study of droplets and particles of different shapes. We do not have this information at this point. That is why considered the case when the angle was constant using the assumptions taken in this research. Given $\vec{f}_{WFM}$, the momentum equation takes the form:

$$\frac{\partial}{\partial t}(\rho \vec{u}) + \nabla \cdot \left(\rho \vec{u} \otimes \vec{u} - \vec{T}\right) = \rho \vec{g} + \vec{f}_\sigma + \vec{f}_{WFM}. \tag{9}$$

Since the free surface moves with the liquid, the motion of the free interface is tracked by solving the volume fraction advection equation in the cell. The volume fraction equation takes the following form:

$$\frac{\partial F}{\partial t} + \nabla \cdot \left(\vec{u} F\right) = 0. \tag{10}$$

The above equations (8)-(10) were solved in the commercial package of Ansys Fluent. The distinguishing feature of the hybrid of Level Set and VOF method is that a single momentum equation is solved for the two phases (gas/liquid). In each cell, the fluid properties are determined according to the volume fractions of the liquid and gas phase from Equations (11) and (12):

$$\mu = \mu_1 \cdot F + \mu_2 \cdot (1 - F). \tag{11}$$

$$\rho = \rho_1 \cdot F + \rho_2 \cdot (1 - F). \tag{12}$$

The hybrid of Level Set and VOF method were coupled in the Fluent software using the approach described below. The surface tension term $\vec{f}_\sigma$ in the momentum equation is a surface force, which is converted into a volume force by the continuum surface force (CSF) model based on the approach of Brackbill et al. [64]:

$$\vec{f}_\sigma = \sigma \kappa \delta(\theta) \vec{n}, \tag{13}$$

where σ is the liquid surface tension, κ is the interface curvature of the free surface and $\vec{n}$ is the normal unit vector at the interface. The Dirac-delta function (δ) guarantees that the surface tension force is only calculated at the interface and is zero everywhere else, in contrast with Volume of Fluid and Level Set separately (14). The surface curvature κ and the surface tension force $\vec{f}_\sigma$ associated with it are calculated more precisely. The value of θ is positive in the gas phase $(+\varepsilon)$, negative in the liquid phase $(-\varepsilon)$, and zero at the interface.

$$\delta(\theta) = \begin{cases} \dfrac{1 + \cos\left(\dfrac{\pi\theta}{a}\right)}{2a}, & |\theta| < a \\ 0, & |\theta| < a \end{cases} \tag{14}$$

where a is the interface thickness and is considered to be $1.5\Delta x$, in which Δx is the grid spacing. Transient solution of both the volume fraction parameter and level set function was calculated using the general advection equation (15):

$$\frac{\partial \theta}{\partial t} + \vec{V} \cdot \nabla \theta = 0. \tag{15}$$

For implementing the numerical simulation, the coupled level set and volume of fluid method was used in ANSYS Fluent 2020 R2. A 2D axisymmetric model was created. All the calculations took gravity effects into account. The calculated physical geometry of the model with an initial mesh consisted of 13,237 elements and 7,280 nodes. In the course of the calculation, the number of elements grew to 500,000 and more due to the adaptive mesh refinement when the shape of a droplet changed and secondary fragments were formed. We ensured that the solutions remained unaffected by the mesh size during the qualitative comparison with the experimental findings below minimum values. In addition, an additional test calculation (Supplementary material D) was carried out for a qualitative comparison of the results of this simulation with the data of 2D planar simulations from [58]. Dynamic mesh refinement allowed the reduction of the mesh size near the interface. A dynamic refinement procedure was implemented every five time steps to decrease the mesh size according to the phase gradient like in [23]. A local mesh refinement was utilized to split the cells up to 3 times. Also, a variable time step was used for more precise calculations. The variable time step used in simulations was determined such that the value of the Courant number always remained less than 0.2 [33]. The number of iterations in each time step was fixed to 20 to assure that the solution error would be less than 10^{-6}. Pressure-velocity coupling is achieved by the Fractional step algorithm. Discretization of the momentum flux term is achieved by a second order upwind scheme, while for the time discretization a first-order implicit approach is followed for the momentum equation. The volume fraction equation is solved in an explicit manner at the beginning of each time-step using as an input the velocity values derived during the previous time step. For the volume fraction flux term, the CICSAM discretization scheme is used [65]. With the above computational settings, we obtained the reasonable agreement with the results of our own actual experiments on the non-conventional droplet-particle collision regimes (deposition, separation, and disintegration) and outcomes (number and size of secondary fragments). At least 100 computations were made to construct the regime maps. The regime transition boundaries were refined using the bisection method. The actual value of simulations was in range 100-200 depending on number of refinements.

2.3 Droplet collision regimes

In this research, we determined the droplet-particle collision regimes according to the approach described in Ref. [66]. Shlegel et al. [66] distinguish the following droplet interaction regimes: deposition (DE), separation (SE), and disintegration (DI). During deposition, two colliding droplets merge into one large drop. Separation occurs as a result of two droplets colliding and forming two droplets of different sizes. The disintegration regime is notable for the formation of secondary droplets (also known as satellite or child droplets), so two droplets collide to form three or more droplets. Typical concentration fields of the above regimes are presented in Fig. 3. Note that two approaches of droplet/particle collisions are widely used when plotting an interaction regime map. The first approach distinguishes four droplet/particle collision regimes: bounce, deposition, separation and disintegration. In contrast the second approach distinguishes five droplet/particle collision regimes: fast coalescence, slow coalescence, bounce, stretching separation, and reflexive separation. The main difference between two approaches refer to their appearance history. The first approach is commonly used in practical applications [21]. The second approach is commonly used when detailed physical reasons of collisions are described [1-3].

When Volume of Fluid is used, especially in the 2D arrangement with a limited number of refinement levels, it is important to determine the ratio of the maximum velocity near the droplet-particle interface to the impact velocity. Fig. 4 shows typical velocity vector fields at the droplet-particle interface (R_d = 1.57 mm, R_P = 1.5 mm, U_d = 2.84 m/s, α = 90°). According to the calculations, the maximum values of velocity vectors fell within 7–8 m/s. The U_{max}/U_d ratios were 2–3. The research findings presented in [60, 61] are notable for higher requirements to the calculations using the Volume of Fluid method, including in terms of the number of refinement levels.

In the present research, the modeling results are presented in the form of $B(We)$ regime maps. The Weber number was given by $We = \rho U_{rel}^2 D_0 / \sigma$, and the linear parameter B was written as $B = 2 \cdot b / (D_S + D_L)$. With varying liquid properties (in particular, density and surface tension), as well as droplet-particle size ratio, the relative droplet velocity U_{rel} was varied to obtain the Weber numbers ranging from 0 to 200. The rest of the parameters involved in the Weber number calculations were considered constant. In particular, with varying density of the liquid in the range of 500 to 2000 kg/m³, the droplet and particle radii were taken as 0.5 mm, the surface tension was taken as 0.0727 N/m, and the absolute values of the relative droplet and particle velocity ranged from 0 to 4 m/s.
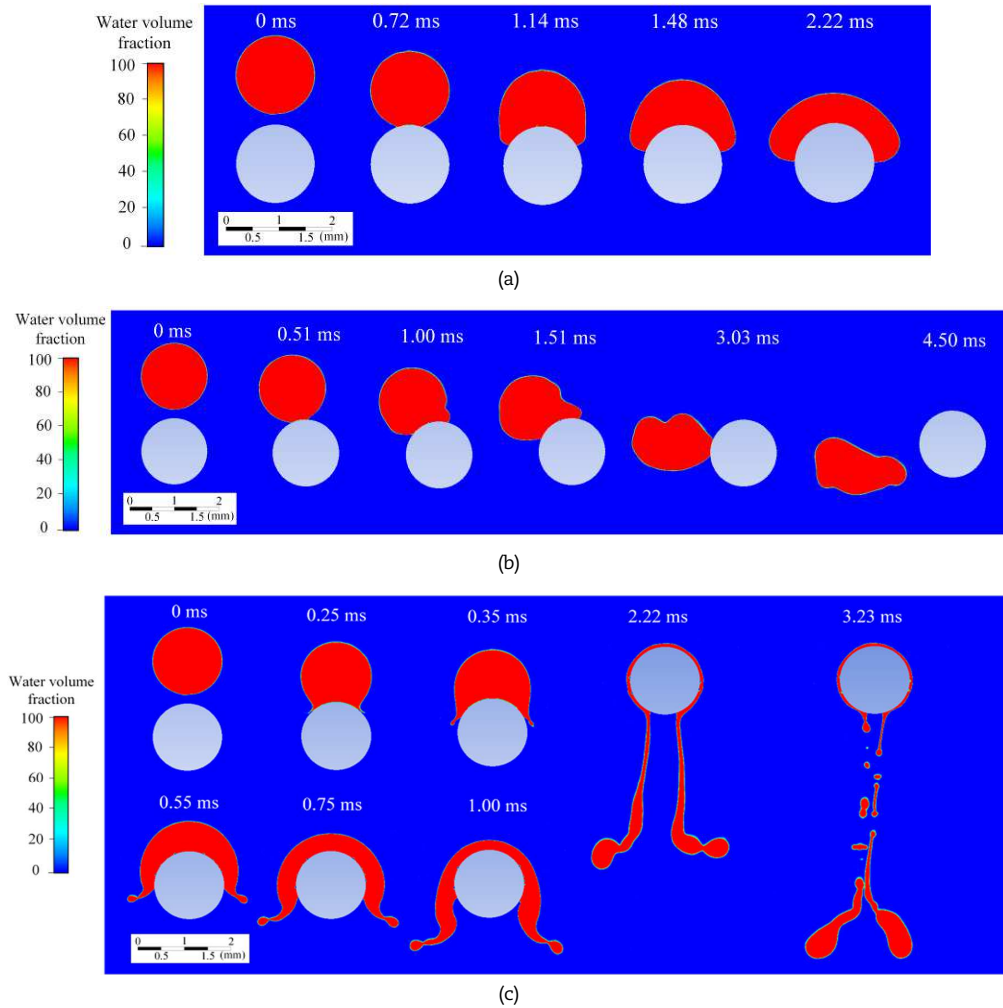
Fig. 3. Typical concentration fields of droplet-particle interaction regimes: (a) – deposition (We=3.6, B=0.002, Δ=1); (b) – separation (We=21.2, B=0.6, Δ=1); (c) – disintegration (We=37.4, B=0.006, Δ=1).

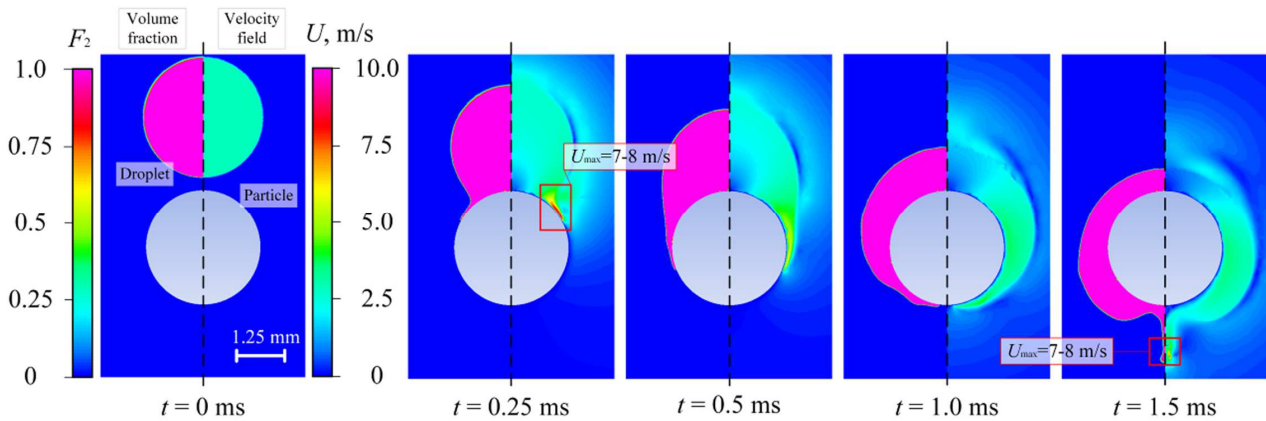**Fig. 4.** Typical velocity vector field at the droplet-particle interface (R_d=1.57 mm, R_p=1.5 mm, U_d=2.84 m/s, α=90°).

We chose coal particles for this research because they are actively used as part of composite liquid fuels, for instance, coal-water slurries with or without petrochemicals. As a rule, the size of coal particles in the corresponding systems ranges from hundreds of micrometers to several millimeters. Particles may also vary in shape (polyhedrons, ellipsoids, spheres, etc.) depending on the coal processing technology. That is why we varied the particle shape (sphere, cube, and octahedron) as part of the simplified approach to the simulation of droplet-particle collisions. A combination of regular shapes studied in this research will be a step to more complex real geometries of coal particles (polyhedrons, ellipsoids, octahedrons, tetrahedrons, etc.).

The kinetic energy, surface energy and energy dissipation during droplet-particle interactions were quantified in [67, 68]. In particular, the ratio of kinetic energies during the interactions between droplets and particles was found to approximate 0.5 [67, 68] under the conditions presented in this research. Calculations were also made for particles with hydrophilic and hydrophilic surfaces as well as with polished and rough surfaces. Secondary fragments broke off from a rough surface at a lower Weber number than from a polished particle surface, which led to a 5–10% increase in the ratio of kinetic energies. More accurate values were determined for the ratios of kinetic and potential energies of droplet-particle collisions [67, 68]: 0.53 for polished particles and 0.55–0.57 for particles with hydrophobic and hydrophilic surfaces.
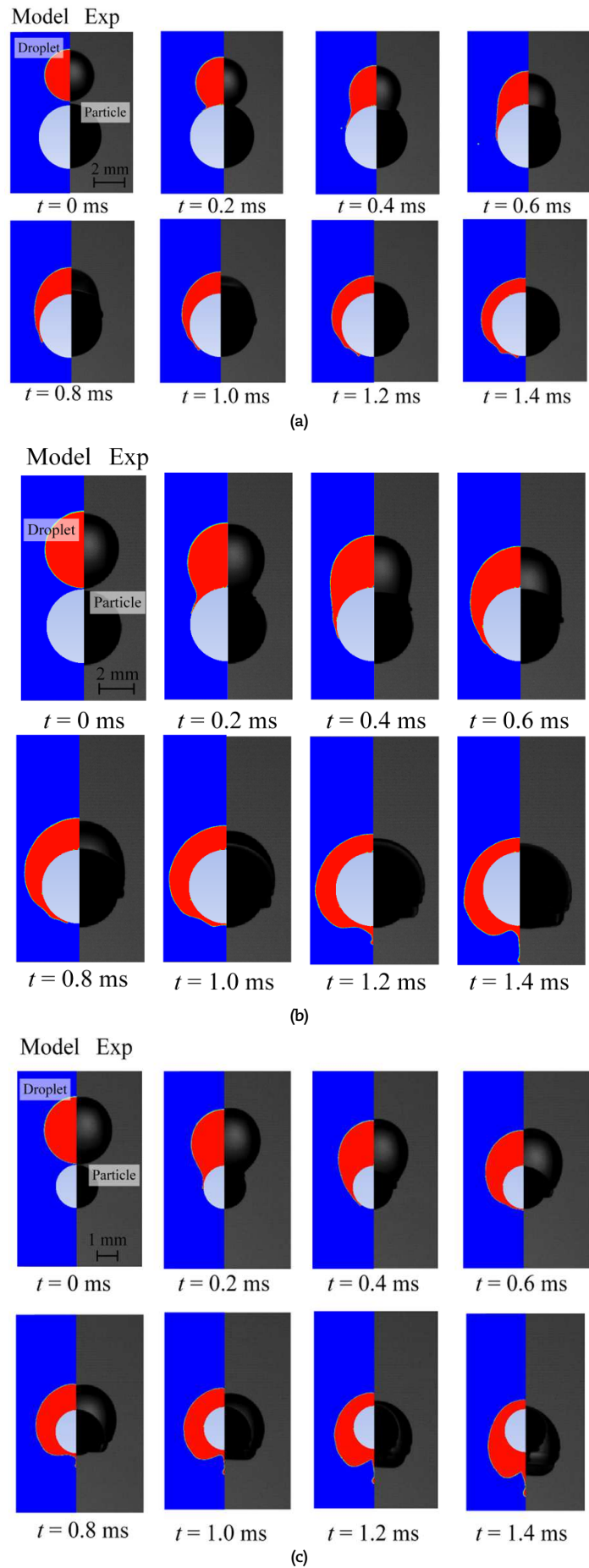
Fig. 5. Snapshots of droplet-particle collisions based on experiments [67] and current simulation: (a) – R_d=1.64 mm, R_p=2 mm, U_d=2.63 m/s, α=90°; (b) – R_d=1.57 mm, R_p=1.5 mm, U_d=2.84 m/s, α=90°; (c) – R_d=1.56 mm, R_p=1 mm, U_d=2.79 m/s, α=90°.

2.4 Model verification

Figure 5 compares droplet-particle collision outcomes in an actual experiment [67] and a model for several initial input parameters. As can be seen from Fig. 5, the droplet-particle collision outcomes are the same, and droplet outlines in the course of deposition are similar in the model and in the actual experiment. Certain differences in the droplet-particle collision outcomes can be attributed to the main assumptions made in the model as well as errors in the measurement of the key parameters in the actual experiment:

i. The model factors out the movement of droplets and particles along the third coordinate (z), which can have a significant impact on their collision behavior. A shift of the centers of mass along the third coordinate during the actual experimental collisions leads to their rotary movement, changes in droplet shapes, collision outcomes, as well as interaction times.

ii. An assumption is made for the calculations that droplets are spherical in shape at the initial point of time. The actual experiments record the deformation of droplet surface as it moves before colliding with a particle.

iii. Experimental errors in the measurement of the location of droplet centers, velocities, and impact angles have a significant impact on the eccentricity of impact and hence on collision outcomes.

iv. Particle rotation is not accounted for when particles collide with liquid droplets.

v. 2D numerical modeling gives a higher droplet spread which can be clearly seen in Fig. 5, but it significantly reduces the computation time compared to 3D modeling [55]. Note that 3D modeling should be taken into account in the cases of quantifying the results of drop/particle collisions [63]. Comparative estimates of the results of 2D and 3D modeling for one of the cases described in the article are presented in Supplementary material E.

vi. The dynamic contact angle is not incorporated in the model, which would make it possible to determine the three phase contact line motion. The corresponding estimates were made in [60–62]. In this work we simulated the collisions between water droplets and solid particles with varying contact angles (60° in Supplementary material A, 90° in Supplementary material B, and 120° in Supplementary material C). Thus we can accurately predict a collision outcome even in simplified mathematical models accounting for the dynamic contact angle as a function of several droplet-particle parameters (interaction time, properties of liquid and particle material, temperature of the gas, droplets, and particles, etc.).

3. Results and Discussion

Fig. 6 presents the collision regime maps based on the obtained simulation results accounting for the density of the liquid. Clearly, the deposition area decreases and the separation area increases with an increase in density because the Weber number directly depends on the density of the liquid. The higher the value of this parameter while the rest of the parameters remain constant, the higher the Weber number. Separation and disintegration require less kinetic energy (relative droplet velocity is lower). Fig. 7 presents the number of secondary droplets versus the Weber number with varying liquid density: $1 - \rho = 2000 \text{ kg/m}^3$; $2 - \rho = 1000 \text{ kg/m}^3$; $3 - \rho = 500 \text{ kg/m}^3$.

There are not enough data in the modern literature describing how varying liquid density affects the collision behavior of liquid droplets, so it is difficult to find out how well the results obtained in this work agree with other authors' findings. An increase in the liquid density leads to an increase in the inertial forces acting on a droplet. As the mass of liquid increases, so does the momentum transferred from the droplet to the particle as a result of their collision. Hence, liquids with greater density need lower impact velocity to reach the conditions of intense disintegration.

Fig. 8 shows the collision regime maps accounting for the impact of the liquid viscosity. With an increase in viscosity, the deposition and separation area increases while the disintegration area decreases. This happens because droplets of more viscous liquids maintain their spherical shape with an increase in velocity, and the contact area between the droplets remains the same at high velocities. In addition, Fig. 9 presents the recorded number of secondary droplets versus the Weber number with varying liquid viscosity: $1 - \mu = 0.01 \text{ Pa·s}$; $2 - \mu = 0.00101 \text{ Pa·s}$; $3 - \mu = 0.0001 \text{ Pa·s}$. According to the calculations, droplets of more viscous liquids break up at higher critical Weber numbers. Moreover, secondary droplets of more viscous liquids maintain their spherical shape after colliding with a solid particle.
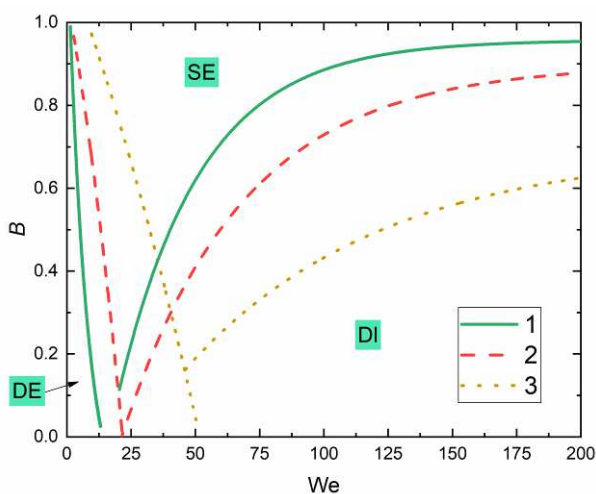

Fig. 6. Collision regime maps based on the impact of liquid density: $1 - \rho=2000 \text{ kg/m}^3$; $2 - \rho=1000 \text{ kg/m}^3$; $3 - \rho=500 \text{ kg/m}^3$.
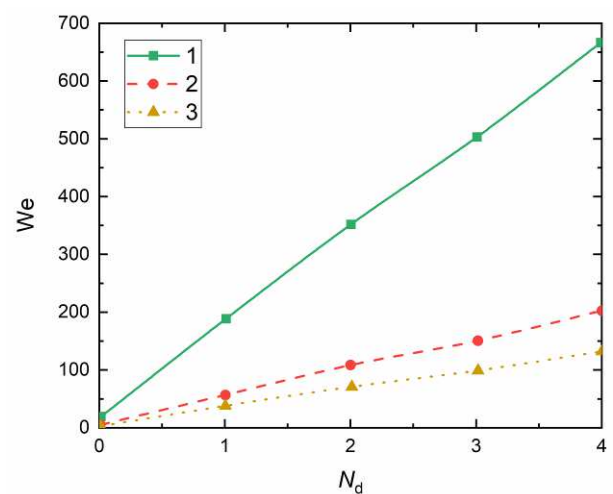
Fig. 7. Number of secondary fragments versus Weber numbers with varying liquid density: $1 - \rho=2000 \text{ kg/m}^3$; $2 - \rho=1000 \text{ kg/m}^3$; $3 - \rho=500 \text{ kg/m}^3$.
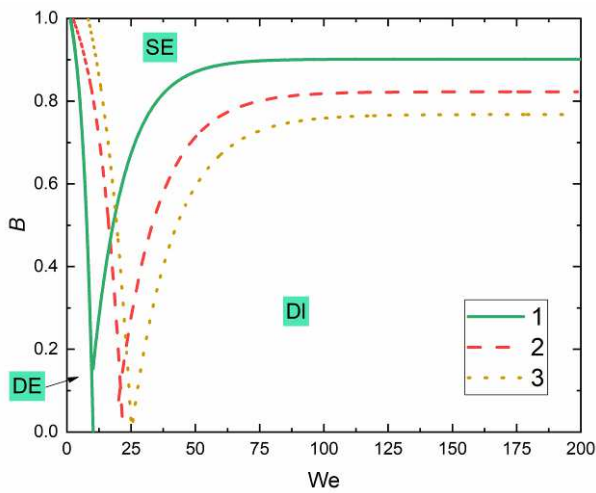
Fig. 8. Collision regime maps based on the impact of liquid viscosity: 1 – μ=0.0001 Pa·s; 2 – μ=0.00101 Pa·s; 3 – μ=0.01 Pa·s.

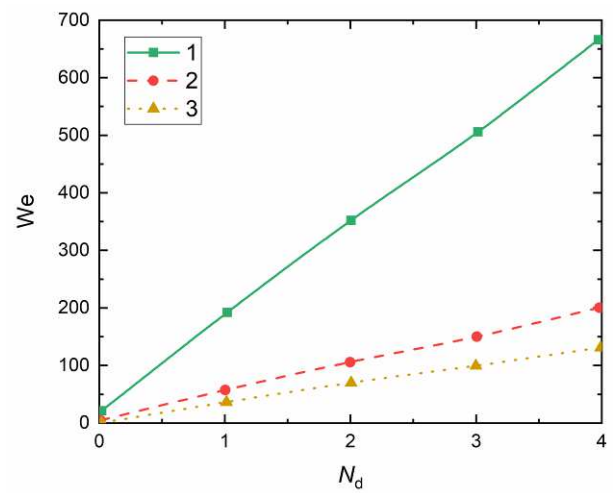**Fig. 9.** Number of secondary fragments versus Weber numbers with varying liquid viscosity: 1 – μ=0.01 Pa·s; 2 – μ=0.00101 Pa·s; 3 – μ=0.0001 Pa·s.
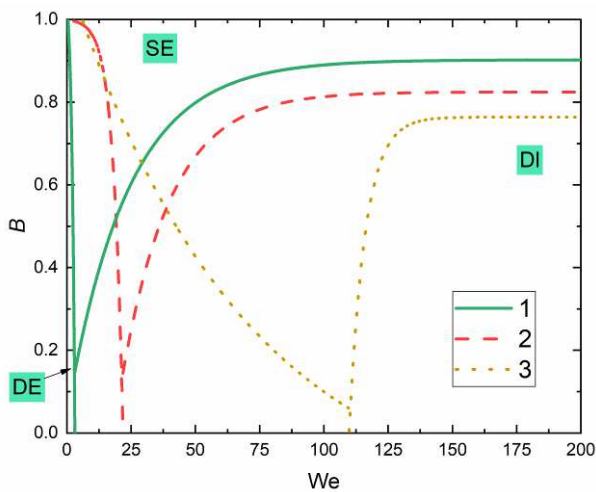

Fig. 10. Collision regime maps based on the impact of liquid surface tension: 1 – σ=0.007 N/m; 2 – σ=0.07269 N/m; 3 – σ=0.7 N/m.
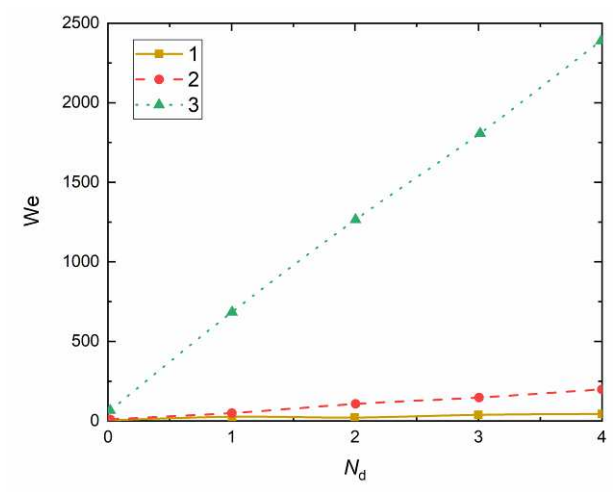

Fig. 11. Number of secondary fragments versus Weber numbers with varying liquid surface tension: 1 – σ=0.007 N/m; 2 – σ=0.07269 N/m; 3 – σ=0.7 N/m.

The ability of a liquid to resist tangential forces in a flow increases with an increase in viscosity. As a result, a considerable portion of kinetic energy is dissipated in the liquid film, and a droplet does not spread as much on the liquid surface [69] (i.e., the average velocity of the liquid flow in a film decreases). The remaining kinetic energy is not enough for the movement of liquid layers relative to each other, and hence it is not enough for the formation of a thin film and its subsequent destruction. Similar results were recorded in [23, 50, 52]. As Banitabaei and Amirfazli reported [23] for highly viscous liquids (μ = 0.35 Pa·s), the post-impact kinetic energy is not enough for the formation of a lamella. In the case of even higher viscosities, the particle gets trapped inside the droplet (the droplet fully envelops the particle). The droplet-to-particle diameter ratio does not affect the collision outcomes. The results obtained in [50] show that when droplets of highly viscous blends collide with a solid particle, the lamella does not disintegrate but just drains in the direction of gravity. For low viscosity liquids, when the impact velocity is high enough, the contribution of viscous forces can be neglected. An increase in viscosity also leads to a reduction in droplet spreading on the particle surface [52]. Also, secondary droplets formed after the collision of a more viscous liquid with a solid particle are larger in size and take the spherical shape faster. This happens because viscous forces dominate over the strain energy in droplets, thus shortening the deformation cycles of secondary droplets and causing changes in their size [70].

Figure 10 presents the collision regime maps accounting for the impact of the liquid surface tension. With a decrease in the surface tension, the separation and disintegration area increases, while the deposition area decreases, because the surface tension of a liquid is inversely proportional to the Weber number with all other properties of the liquid being constant. Liquid droplets with lower surface tension require lower velocity to break up. In addition, Fig. 11 shows the numerically obtained number of secondary droplets versus the Weber number with varying surface tension of a liquid: 1 – σ = 0.007 N/m, 2 – σ = 0.07269 N/m, 3 – σ = 0.7 N/m.

Surface tension has a considerable impact on the fragmentation of liquid droplets colliding with solid particles. A reduction in surface tension weakens the forces keeping the near-surface liquid layers in place. As a result, the near-surface layers of a droplet impinging on a solid surface break up quickly into secondary droplets. The latter deviate more from the spherical shape, and their deformation cycles become longer. This suggests that a decrease in the surface tension leads to a decrease in the threshold values of inertial forces required for the breakup of liquid droplets (i.e., lower critical droplet velocities are enough for critical Weber numbers) [70]. The research findings by other authors show similar trends: the greater the ratio of inertial forces to surface tension, the easier it is to destroy a droplet [1, 21, 71]. Also, since the droplet deformation due to the impact is reversely proportional to the surface tension coefficient [69], a droplet with a higher surface tension coefficient will be less deformed when impinging on a solid surface [72].

Figure 12 shows the numerically obtained droplet-particle interaction regime map with varying particle-to-droplet size ratio $\Delta=D_s/D_L$. The calculations were made with a constant water droplet size $R_d=0.5$ mm. It was assumed for the calculations that particles were stationary and spherically shaped. Figure 13 gives a diagram of the average number of secondary liquid fragments formed by the collision between water droplets and different-sized coal particles for five ranges of the We number. Figures 12 and 13 show that an increase in the solid particle size leads to a significant increase in the disintegration area, an increase in the deposition area, and a decrease in the separation area. These findings result from the increase in the contact area between droplets and solid surface during collisions. Consequently, at low Weber numbers, droplet-particle collisions produce more fragments at lower particle-to-droplet size ratio. The larger the contact area during impact, the lower the probability of separation. This regime occurred in the case of a grazing droplet-particle collision. The interaction time was relatively short, and no secondary droplets were formed as a result.   The larger part of a droplet usually continued moving while the smaller part of the liquid stuck to the particle surface. The droplet velocity during separation was rather high, so the conditions for deposition were not achieved. With larger particles, deposition occurred even at high values of the dimensionless linear interaction parameter B (non-coaxial droplet collision) because of the longer droplet-particle interaction time. At higher We numbers, disintegration occurred for the same reason. With an increase in the Weber number, the number of secondary fragments also increased for all the size ratios. This value went up with an increase in the particle-to-droplet size ratio. Fig. 14 shows the actual experimental results [21] of varying the size of a bituminous nonbaking coal particle with $0.5<R_p<0.75$ mm and $0.25<R_p<0.5$ mm (i.e. $\Delta\approx1.5$ and $\Delta\approx1$ respectively) colliding with water droplets. The deposition regime was observed for the particles with $R_p<0.25$ mm ($\Delta\approx0.5$). With other particle-to-droplet size ratios, the separation area increased with an increase in the particle size. This happened because the particle-to-droplet size ratio was close to 1 at $0.25<R_p<0.5$ mm and their contact area was bigger than at $0.5<R_p<0.75$ mm. Since the distance between the centers of mass increased in the latter case, the kinetic energy was partially spent on particle rotation. As a result, it was not enough to overcome the viscous force. Therefore, the disintegration boundary shifted towards higher critical Weber numbers. The particle rotation also caused the droplet to separate from the particle surface instead of merging with it. The rotation of the moving particle is the main reason why the findings obtained experimentally differ from the numerical simulation results. This factor has a significant impact on the deposition and disintegration regime boundaries. The newly developed model does not reflect the rotational kinetic energy of the solid particle. As a result, the rotation-induced separation of the droplet from the solid surface is not addressed either.
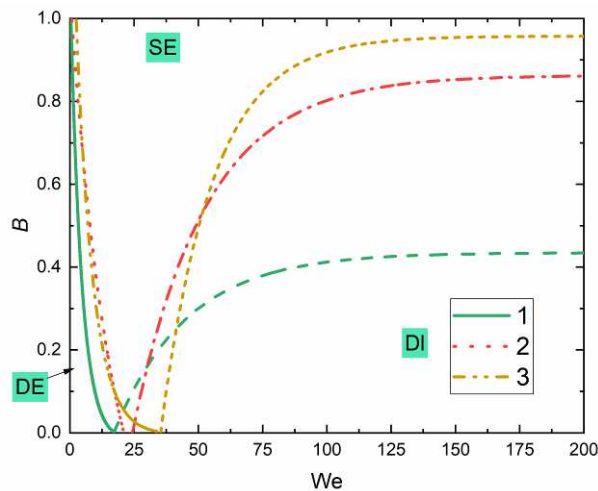

Fig. 12. Comparison of the interaction regime boundaries for water droplets colliding with spherical solid coal particles for different size ratios: $1 – \Delta=0.5$; $2 – \Delta=1$; $3 – \Delta=1.5$.
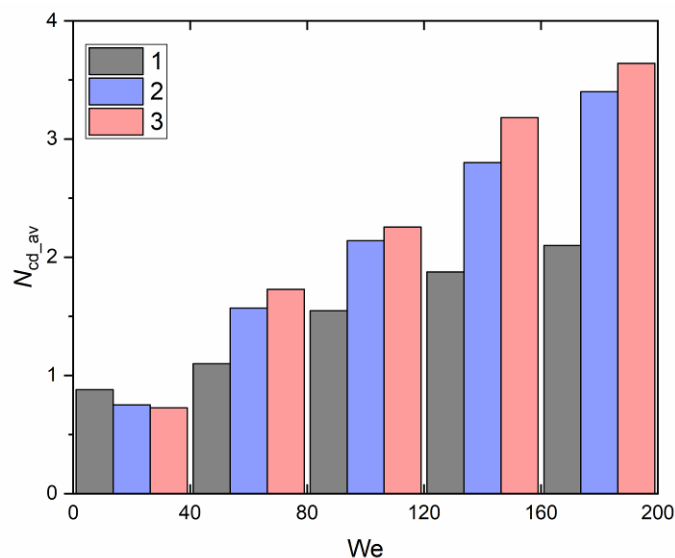

Fig. 13. Average number of secondary droplets formed after collisions between water droplets and solid particles for different size ratios: $1 – \Delta=0.5$; $2 – \Delta=1$; $3 – \Delta=1.5$.
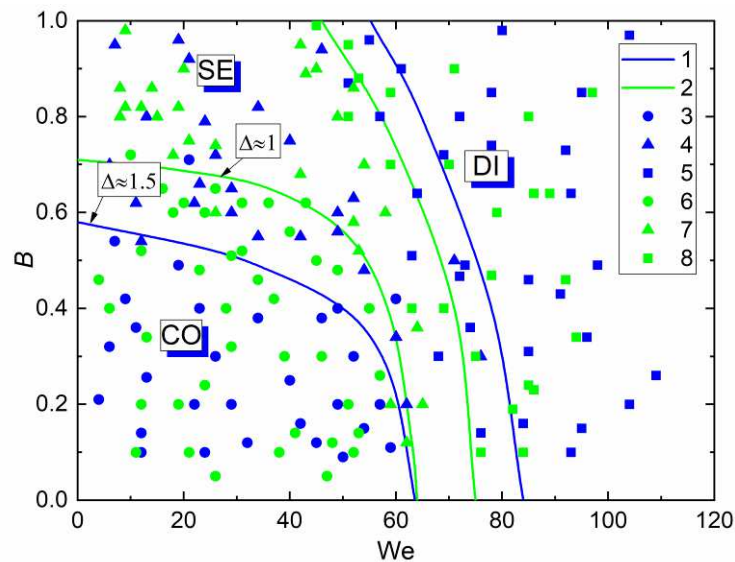
Fig. 14. Experimental interaction regime map [21] for water droplets and low-caking coal particles obtained using the linear interaction parameter: 1 – 0.5<R_p<0.75mm; 2 – 0.25<R_p<0.5 mm; 3, 6 – deposition; 4, 7 – separation; 5, 8 – disintegration.

This research did not take into account the rotation of a solid particle. The particle was stationary. As a result of collision, the kinetic energy supplied from the droplet to the particle was not spent on rotation. The particle had a zero momentum throughout the interaction time. The main aim of this research was to study the non-conventional droplet-particle collision outcomes (deposition, separation, disintegration), which are important for the development of practical applications based on intense atomization of liquid droplets.

Figure 15 shows the interaction regime map for water droplets colliding with stationary solid particles of different shapes. The size ratio was Δ=1 at all times. Figure 16 presents the average number of secondary droplets formed after the collision of water droplets with coal particles of different shapes for five ranges of the We numbers. Figures 15 and 16 show that the disintegration area on the collision regime map increases when the particle shape changes from a sphere to a cube. Moreover, the deposition boundary shifts towards higher values of the dimensionless linear interaction parameter. This can be attributed to an increase in the contact area between the water droplet and the solid surface. Sharp edges of the cube also play an important role: they favor the breakup of a thin liquid film in this area when a water droplet flows over a solid particle. With a switch from the cubic shape to an octahedron, the deposition area decreases because the liquid slides on an inclined surface. At the same time, the boundary between the separation and disintegration shifts towards lower values of We and B. When the particle shape is changed from a sphere to a cube or an octahedron, the number of secondary droplets increases due to the expanding disintegration area. At low Weber numbers, the greatest number of satellite droplets is formed from the collisions with octahedron-shaped particles, whereas at high Weber numbers, it is the interaction with cube-shaped particles that produces the greatest number of secondary droplets.

Typical snapshots of droplet-particle collisions based on theoretical calculations for three particle shapes (sphere, cube, and octahedron) are shown in Fig. 17. The analysis of the interaction between droplets and particles of different shapes (sphere, cube, and octahedron) will make it possible to take on a more complex and detailed analysis of irregular shapes inherent in coal particles [73, 74], which are considered in this research and are widely used in various energy-related applications. Fig. 18 presents the experimentally obtained interaction regime map [21] for water droplets colliding with brown coal particles of different shapes. It shows how the shape of solid particles affects the particle-droplet interaction regime boundaries. Cylindrical particles have a more round and uniform surface without any sharp edges, while being of approximately the same average size as polyhedron particles. Thus, the surface area of cylindrical coal particles was smaller than that of polyhedrons. The numerical simulation results are consistent with the actual experimental findings in terms of the decrease in the separation area and extension of the disintegration area when the particle shape changes from a sphere to a polyhedron. The comparison of the regime maps numerically simulated using a simplified numerical simulations against the actual experimental findings can help improve the simulation of droplet interactions with particles of complex geometry. Switching to the 3D modeling arrangement should be given special attention. This way it will be possible to consider in greater detail the droplet collisions with particles of both regular shapes (sphere, cube, and octahedron) and irregular, highly asymmetrical shapes [55]. In addition, it is important to take into account the dynamic contact angles as a function of the droplet-particle interaction time [60–62], especially for non-spherical particles and droplets [75].

The analysis of droplet-particle behavior has revealed significantly different dynamic characteristics, in particular, the rates of liquid spreading on the surface and contact areas (Fig. 17). These rates define the shear behavior of liquid layers and the ratio of the kinetic and surface energy in the collision zone. The sharper the edge of an octahedral particle, the faster the liquid spreads when a droplet contacts the particle. The slowest spreading is observed in the case of cylindrical particles. In real technologies, particles are polyhedral and ellipsoidal, so the spreading rates will be average relative to a sphere and octahedron. As a result, the thicknesses of the liquid films forming on a solid surface are different, which affects the collision outcomes for subsequent impinging droplets. The more sharp edges are particle has, the more liquid drains to the lower part of the particle and breaks off from its surface. The results of numerical simulations presented in this work can be used as the upper and lower boundaries of the possible variation ranges for the Weber number and linear and angular impact parameters, sufficient for the transition from one regime to another. The model can predict the number and size of the emerging secondary liquid fragments, as well as their shapes, trajectories, and velocities.
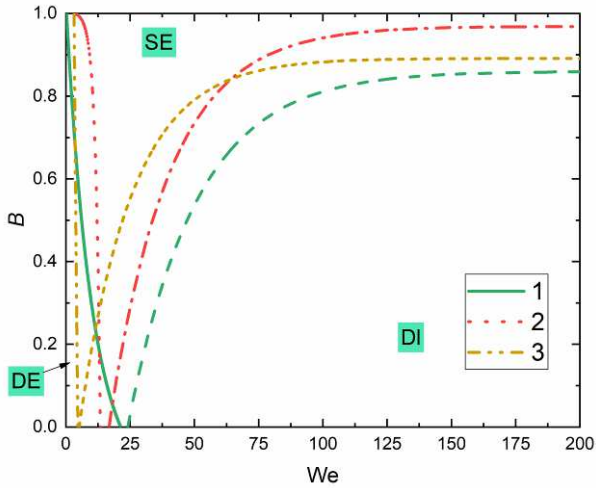
Fig. 15. Comparison of the interaction regime boundaries for water droplets colliding with solid coal particles of different shapes: 1 – sphere; 2 – cube; 3 – octahedron.
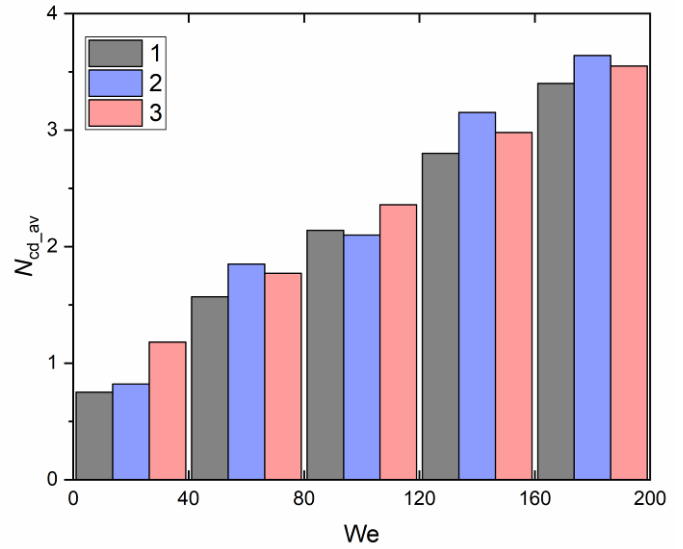

Fig. 16. Average number of secondary droplets formed after collisions between water droplets and solid particles of different shapes: 1 – sphere; 2 – cube; 3 – octahedron.
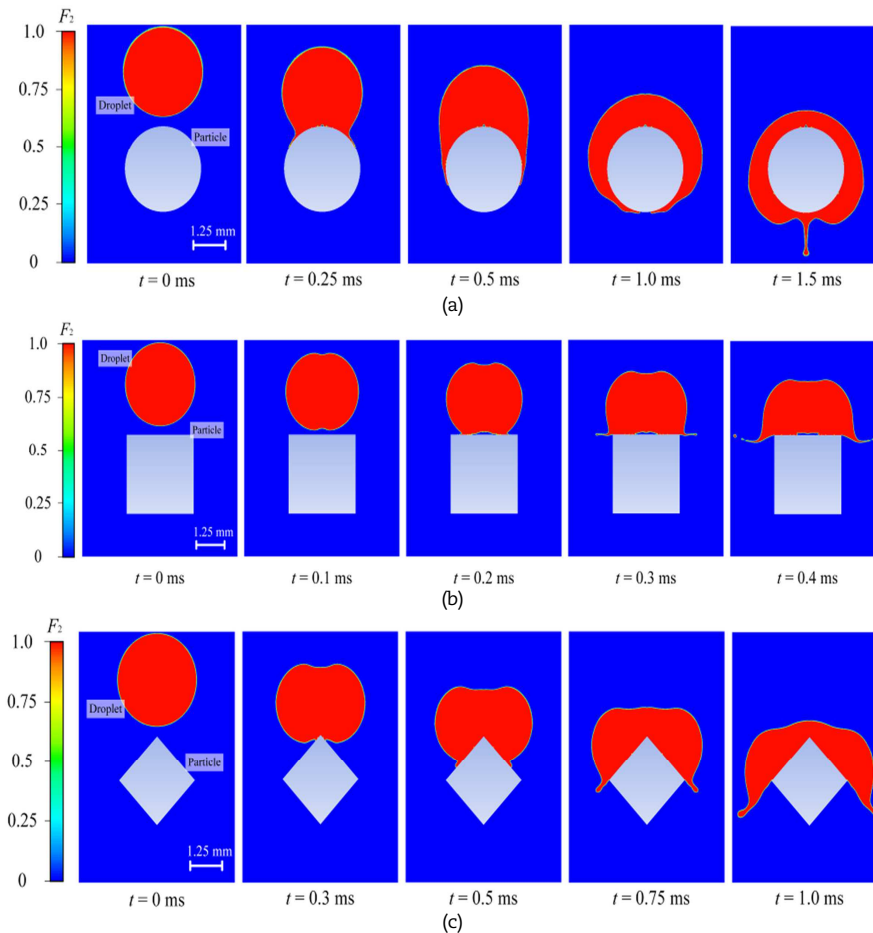

Fig. 17. Snapshots of droplet-particle collisions based on theoretical calculations: (a) – sphere; (b) – cube; (c) – octahedron.

The droplet-particle size ratio has a paramount impact on their collision outcomes. With the particle and droplet of equal size, two regimes specified on the map (Fig. 18) can occur stably depending on the resultant velocity. However, if the droplet is significantly smaller than the particle, the liquid spreads on a solid surface in a wide variation range of the resultant velocities. Otherwise a droplet envelops the particle and breaks off from its surface, i.e., a solid particle pierces through the droplet. The higher the resultant velocity, the more liquid breaks off from the solid surface. The larger the droplet-particle contact area and the smaller the impact angle, the greater volume of the droplet remains on the particle surface. The modeling results have shown that these characteristics can be successfully controlled and varied in wide ranges. At the same time, when the droplet-particle size ratio is below 0.3, one can use the modeling approaches developed for studying the droplet impingement on a massive solid wall [62, 76]. With such size ratios, a droplet spreads on a particle surface and remains on it despite different arrangements. Only when the resultant velocities exceed 10 m/s, droplets start to break off consistently from the particle surface. However, these

critical conditions can also be described using the known models of droplet collisions with massive walls. Thus, here we have determined the conditions in which it is important to use special-purpose models simulating droplet collisions with solid particles and general models of droplet interaction with a massive solid wall that is significantly larger than the droplet and the particle.

The dynamics of the liquid droplet surface deformation when colliding with a solid particle (Fig. 17) with varying velocities and size ratios indicates that interesting joint (synergistic) effects manifest themselves when several droplets and particles collide simultaneously [75]. In particular, the droplet-particle size ratio, the particle surface geometry, and the resultant velocity determine the transversal and longitudinal size of the complex *droplet-particle* system during interaction. With similar systems located at a distance of several radii from each other, they will have a mutual influence on their deformation. The more facets a particle has, the more considerable the joint influence will be. Clearly, this influence will be even more significant if the droplet and particle surface deformation is taken into account before collision, i.e., during their motion in a gas. These conditions are difficult to reproduce in a model, given the multitude of factors and effects. They would be interesting to study as part of further actual experimental research using tracking software and hardware packages. The particle shape defines the aerodynamic forces acting on the particle from the oncoming gas or liquid flow. The so-called traces (regions in the flow behind the particles) differ significantly [77]. This same factor defines the transversal and longitudinal sizes of the corresponding aerodynamic traces when liquid droplets collide with particles of various shapes. That is why, when it comes to a group of droplets hitting the same particle one after another, the proposed model can predict both the collision outcomes (regime and number of secondary fragments) and the overall characteristics of the gas zone behind the particle surface [77].

The analysis of spray applications involves real shapes (ellipsoids and polyhedrons) of particle surfaces and significant difficulties associated with the simulation of collisions between different-shaped particles and droplets, especially as part of a spray [75, 78, 79]. As a rule, the particles are assumed to be spherical in the models. If the particles have a given shape, for instance, when prepared on a conveyor belt, one can choose a specific collision scheme (Fig. 17) to predict the interaction regimes. In the case of several particles of different shapes (i.e., without separating them into spheres, ellipsoids, and polyhedrons), the data obtained can be used as the basic boundaries for some regions of scatter in the values of the key interaction parameters for real applications involving particles of different shapes (tetrahedrons, polyhedrons, ellipsoids, etc.). The data used in this research can be used to predict the collision behavior even for convex and concave bodies, because the greatest difference in the droplet breakoff from a solid particle is observed when considering a sphere and an octahedron. Figs. 15 and 18 demonstrate the essential difference between actual experiment and numerical simulation in 2D concept. Note that in the future it is important to consider the tasks of detailed 3D modeling of the collision of droplets and particles of various shapes within the framework of separate research.

Figure 19 shows the interaction regime map for water droplets colliding with solid particles of different densities. We used particles of two coal ranks: bituminous nonbaking coal with $\rho=1340$ kg/m^3 and brown coal with $\rho=1150$ kg/m^3. The particles were assumed to be cylindrical in shape. Fig. 20 shows the average number of secondary droplets formed after the collision of a water droplet and a coal particle for five ranges of the We numbers with varying solid particle density. Figs. 19 and 20 show the effect of the density of particles colliding with water droplets on their interaction regime. The analysis of Figs. 19 and 20 suggests that this parameter can be considered negligible in the problem statement where a particle is stationary and its surface has no pores or protrusions.

Figure 21 presents the interaction regime maps for water droplets colliding with solid particles with varying surface wettability. In the calculations, we varied the contact angle for the nonbaking, brown, and low-caking coals. The contact angles for the coals of these three ranks were obtained experimentally using the statistical contact angle method and equaled 74.4°, 97.2°, and 98.4°, respectively. The particles were assumed to be stationary and cylindrical in shape. According to Fig. 21, the deposition boundaries shift towards greater Weber numbers with a decrease in the contact angle and, hence, an increase in the particle surface wettability. Water droplets stick better to a more hydrophilic surface. The deposition area expands to cover the whole range of the parameter B. At the same time, the critical Weber numbers, at which deposition takes place, increase in the range of $22 < We < 28$. With an increase in the hydrophilic properties of the particle surface, the disintegration area also expands towards higher values of the dimensionless linear interaction parameter ($0.88 < B < 0.95$). However, the boundary of this area with respect to We remains practically the same. The analysis of Fig. 21 shows that water droplets stick to nonbaking coal particles better than to brown or low-caking coal fragments at low Weber numbers (< 30). At high Weber numbers (> 50) and high values of the parameter B, better surface wettability leads to the formation of more satellite fragments from the near-surface layer of the liquid film.
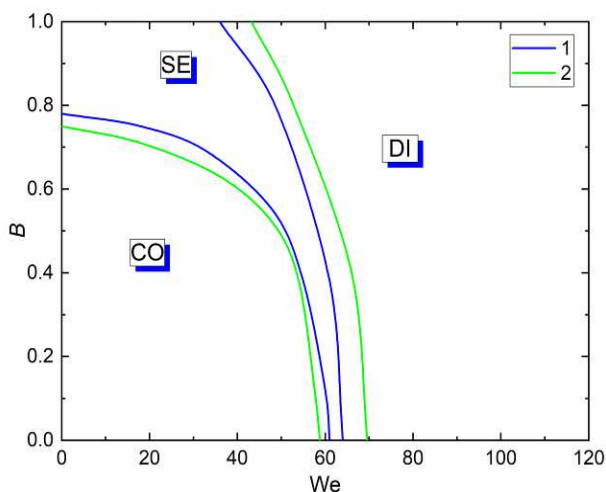

Fig. 18. Experimental interaction regime map [21] for water droplets colliding with brown coal particles $0.25<R_p<0.5$ mm of different shapes: 1 – polyhedron; 2 – sphere.
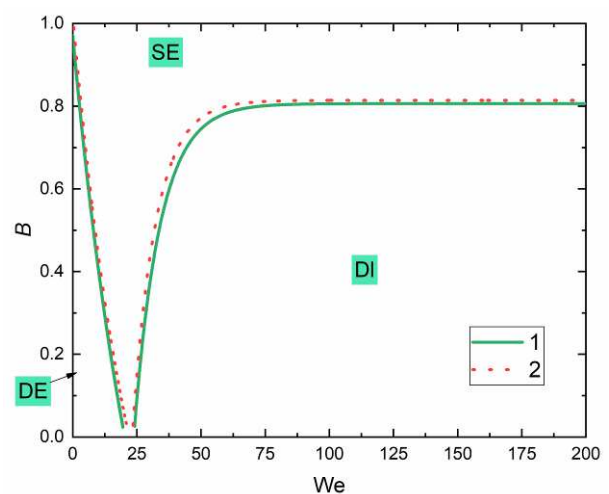

Fig. 19. Interaction regime map for water droplets colliding with solid particles of different densities: 1 – $\rho=1340$ kg/m^3; 2 – $\rho=1150$ kg/m^3.

With lower hydrophilic properties of the particle, the droplet interacts with its surface much more weakly. Figure 22 presents the diagram of the average number of secondary droplets formed after a droplet-particle collision for five ranges of the We numbers. For coals of all the ranks, the number of secondary droplets is shown to double in the range of We from 0 to 160. At the same time, the more hydrophilic the particle was, the more secondary droplets were formed. This happened because less liquid settled on the particle surface when a droplet broke up as a result of a collision. Due to the hydrophilic properties, large water fragments bounced off the surface, which caused the formation of more satellite droplets. A reverse trend was established at Weber numbers above 160: the greater the droplet wettability was, the more secondary droplets were produced. With an increase in the hydrophobic properties, a fast-moving droplet interacts with the particle surface very weakly, hence the grazing droplet-particle collision (i.e., separation) at high values of the parameter B (> 0.8). With an increase in the hydrophilic properties, however, a droplet sticks to the particle surface even under such conditions. A thin liquid bridge is formed and breaks up to form an array of secondary droplets. In the actual experiment [21] (Fig. 23), droplet breakup was observed in the range of $60 < We < 80$ at $B < 0.6$. When the impact was less head-on ($B > 0.8$), the critical Weber numbers shifted to the left to fall into the range of 35–45 depending on the coal rank. Deposition was observed in the case of $B < 0.8$ for all the coals when the Weber number ranged from 45 to 60. It was established that when water droplets were broken by the nonbaking coal particles, the critical Weber number was at its maximum (about 75). This is linked to the hydrophilicity of nonbaking coal, which is the highest among all the coals under study. As a result, water wets the coal particle and fills its pores, thus holding on the surface. With a decrease in the hydrophilic properties, the disintegration regime boundary shifts to lower critical Weber numbers (e.g., about 70 for brown coal and about 62 for low-caking coal). The same situation is observed for the deposition of water droplets and coal particles. The more hydrophilic the coal, the wider range of Weber numbers corresponds to the deposition regime. In particular, the deposition regime is observed in the Weber number range of 0–48 for low-caking coal, 0–58 for brown coal, and 0–63 for nonbaking coal. The comparison of numerical simulation results and actual experimental findings has shown that the deposition area expands with an increase in the hydrophilicity of the particle surface. For the disintegration area, the differences are conditioned by a number of assumptions taken in the model: it factors out the particle translation or rotation as well as the roughness and porosity of the surface.
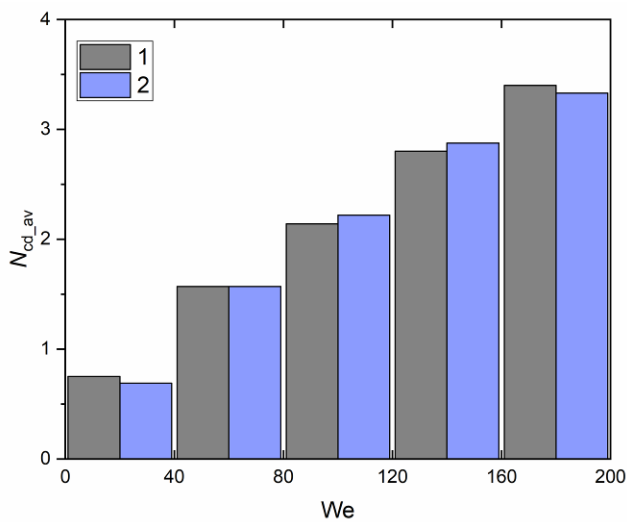

Fig. 20. Average number of secondary droplets formed after collisions between water droplets and solid particles of different densities:
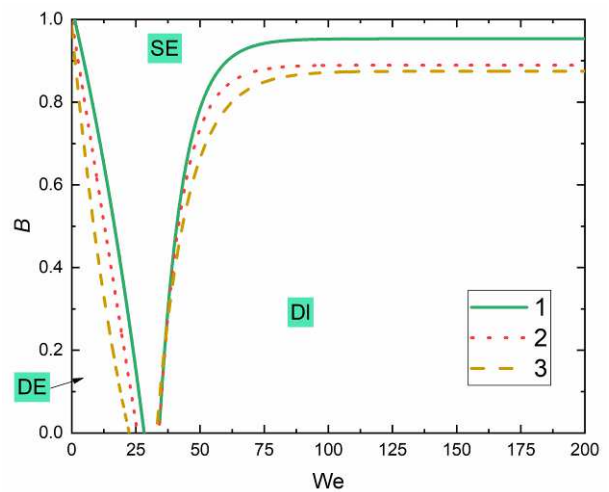1 – ρ=1340 kg/m³; 2 – ρ=1150 kg/m³.

Fig. 21. Interaction regime maps for water droplets colliding with varying surface wettability:
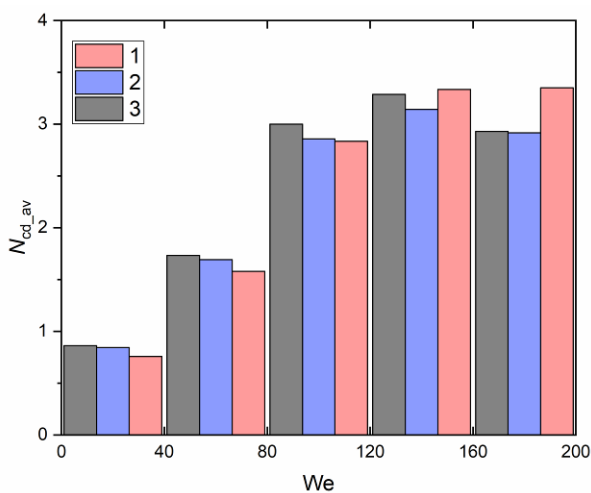1 – bituminous nonbaking; 2 – brown; 3 – bituminous low-caking.

Fig. 22. Average number of secondary droplets formed after collisions between water droplets and coal particles of three ranks:
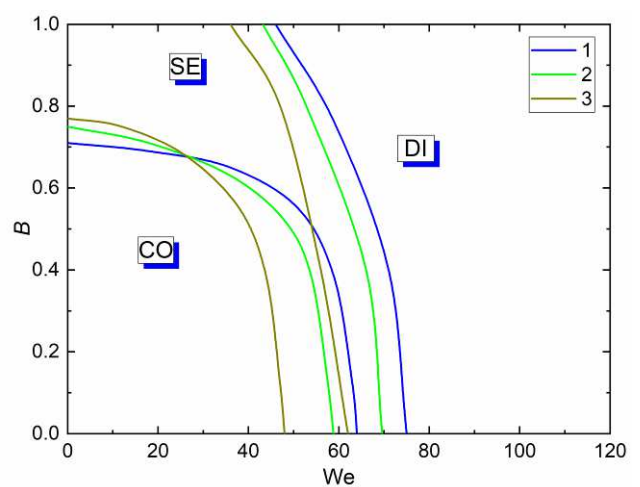1 – bituminous nonbaking; 2 – brown; 3 – bituminous low-caking.

Fig. 23. Experimental interaction regime map [21] for water droplets and coal particles ($0.25<R_P<0.5$) obtained using the linear interaction parameter: 1 – bituminous nonbaking; 2 – brown; 3 – bituminous low-caking.

4. Current Research Findings vs. Previous Evidence

Earlier studies on this topic focused on the impact of viscosity, surface tension, wettability, and droplet-particle size ratio on droplet-particle collision behavior. We would like to underline the following findings of those studies. The wettability of a solid particle (contact angle) affects the droplet-particle collision outcomes and interaction time. A droplet impinging on a hydrophilic particle does not break up or stretch enough to produce a liquid film across the whole velocity variation range (0.05–5 m/s), and the droplet-particle interaction time decreases with an increase in the particle wettability [29]. With an increase in viscosity from 0.001 to 0.35 Pa·s, most of the kinetic energy will be dissipated inside the liquid film. Therefore, in the case of highly viscous liquids (μ = 0.35 Pa·s), the remaining kinetic energy is not enough to move liquid layers relative to each other and create a thin liquid film. The greater the liquid viscosity, the shorter the lamella that is formed. With a further increase in viscosity, a particle may even get trapped inside the droplet [23]. Similar results were obtained by Mitra et al. [50]: for droplets of highly viscous blends, a considerable part of kinetic energy is dissipated, so the lamella does not disintegrate but just drains in the direction of gravity. For low viscosity compositions, when the impact velocity is relatively high, viscous forces can be neglected. Higher viscosity of liquid also reduces droplet spreading on the particle surface [52]. Capillary force plays an important part in droplet-particle collisions as well. It depends on interfacial tension, particle size, and impact angle. If the capillary force is high enough, this upward acting force together with buoyancy may push the droplet from the particle, thus leading to bounce. Conversely, when a droplet collides with a particle at a higher velocity, the downward inertial force is greater than the upward restoring force, which results in complete penetration of the particle into the droplet [51]. The particle wettability also affects collision behavior. For a particle with a contact angle of 90°, a droplet will deposit on the surface, whereas for a hydrophobic particle, the droplet and particle will interact in the bounce regime. When impinging on a hydrophilic particle, a droplet will break up [14].

5. Conclusion

We developed a model for collisions between water droplets and solid particles that accounts for varying parameters of the liquid droplet/solid particle system in a wide range: the density of liquid and the solid particle, viscosity and surface tension of the droplet, the droplet-to-particle size ratio, as well as the shape and type of the solid particle. The results of numerical simulations were presented for droplet-particle collisions in a gas with varying key parameters of the droplet (i.e., its properties and component composition). We showed the impact of density, viscosity, and surface tension on the droplet collision regime maps as well as on the number of secondary fragments. By varying the properties of liquid droplets, one can provide specific droplet-particle collision regimes (deposition, disintegration, or separation) using separated flows of liquid and solid components in real gas-vapor-droplet technologies. It was shown that liquids with greater density, lower viscosity and lower surface tension need lower impact velocity to reach the conditions of intense disintegration. Surface tension had a considerable impact on the fragmentation of liquid droplets colliding with solid particles. A reduction in surface tension weakened the forces keeping the near-surface liquid layers in place. With the use of the regularities obtained, it was possible to control the processes of fragmentation of droplets when interacting with solid particles. The established features on the influence of classical particle shapes (sphere, cube, and octahedron) in drop/particle collisions should be used in predicting more complex and irregular shapes in coal particles. Classical cylindrical solid particles had a more round and uniform surface without any sharp edges. But real sharp of coal solid particles was not cylindrical. In more cases the sharp of coal articles is polyhedron. It leads to an increase in disintegration area in comparison with cylindrical particles. It was observed as in actual experiments as in modeling. These effects should be taken into account at the analysis of coal particles/droplet collisions in real applications especially in boiler units and power plants.

Author Contributions

D.V. Antonov: Conceptualization, Methodology, Resources, Investigation, Software, Writing – original draft. R.M. Fedorenko: Conceptualization, Methodology, Resources, Investigation, Software. P.A. Strizhak: Supervision, Resources, Investigation, Methodology, Writing – review & editing.

Acknowledgments

Conflict of Interest

The authors declared no potential conflicts of interest concerning the research, authorship, and publication of this article.

Funding

Data Availability Statements

The datasets generated and analyzed during the current study are available from the corresponding author on reasonable request.

Nomenclature

B	Linear parameter	T	Temperature [K]
d	Droplet	T_0	Initial temperature [K]
D_0	Initial diameter [mm]	u	Velocity [m/s]
D_L	Diameter of liquid droplet [mm]	$U_{d1(2)}$	Velocity of the liquid droplet (solid particle) [m/s]
D_S	Diameter of solid particle [mm]	U_{rel}	Relative droplet velocity [m/s]
F	Volume fraction	$U_{x(y)}$	Projection of velocities on the $x(y)$ axis [m/s]
f_σ	Surface tension term [N/m^3]	We	Weber number
f_{WFM}	Adhesion stress term (volumetric) [N/m^3]	x, y, z	Coordinates of Cartesian system

g	Gravity acceleration [m^2/s]	α_d	Impact angle [°]
i	Number of phases	Δ	Diameter ratio
p	Particle	κ	Interface curvature [1/m]
$R_{d1(2)}$	Droplet radii of the liquid droplet (solid particle) [mm]	μ	Dynamic viscosity [Pa·s]
Re	Reynold number	ν	Kinematic viscosity [m^2/s]
r_{cd}	Child droplet radii [mm]	ρ	Density [kg/m^3]
S_0	Pre-collision evaporation surface area [mm^2]	σ	Surface tension coefficient [N/m]
S_1	Post-collision evaporation surface area [mm^2]	1	Liquid
t	Time [s]	2	Air

References

[1] Malgarinos, I., Nikolopoulos, N., Gavaises, M., A numerical study on droplet-particle collision dynamics, *International Journal of Heat and Fluid Flow*, 61(B), 2016, 499–509.

[2] Khojasteh, D., Kazerooni, N.M., Marengo, M., A review of liquid droplet impacting onto solid spherical particles: A physical pathway to encapsulation mechanisms, *Journal of Industrial and Engineering Chemistry*, 71, 2019, 50–64.

[3] Yoon, I., Shin, S., Computational study on dynamic behavior during droplet-particle interaction, *Chemical Engineering Science*, 241, 2021, 116656.

[4] Das, S., Panda, A., Patel, H. V, Deen, N.G., Kuipers, J.A.M., DNS of droplet impact on a solid particle: Effect of wettability on solid conjugate heat transfer, *International Journal of Heat and Mass Transfer*, 158, 2020, 119859.

[5] He, P., Wang, D., Zhu, C., Liquid attachment and momentum transfer by collisions between free-fall solids and liquid spray droplets, *Powder Technology*, 239, 2013, 1–11.

[6] Panda, R.C., Zank, J., Martin, H., Modeling the droplet deposition behavior on a single particle in fluidized bed spray granulation process, *Powder Technology*, 115, 2001, 51–57.

[7] Menni, Y., Chamkha, A.J., Ameur, H., Ahmadi, M.H., Hydrodynamic Behavior in Solar Oil Heat Exchanger Ducts Fitted with Staggered Baffles and Fins, *Journal of Applied and Computational Mechanics*, 8(3), 2022, 774–790.

[8] Abdul Gaffar, S., Ramesh Reddy, P., Ramachandra Prasad, V., Subba Rao, A., Khan, B.M.H., Viscoelastic Micropolar Convection Flows from an Inclined Plane with Nonlinear Temperature: A Numerical Study, *Journal of Applied and Computational Mechanics*, 6(2), 2020, 183–199.

[9] Fallah, B., Dinarvand, S., Eftekhari Yazdi, M., Rostami, M.N., Pop, I., MHD Flow and Heat Transfer of SiC-TiO2/DO Hybrid Nanofluid due to a Permeable Spinning Disk by a Novel Algorithm, *Journal of Applied and Computational Mechanics*, 5(5), 2019, 976–988.

[10] Yoon, I., Shin, S., Direct numerical simulation of droplet collision with stationary spherical particle: A comprehensive map of outcomes, *International Journal of Multiphase Flow*, 135, 2021, 103503.

[11] Malgarinos, I., Nikolopoulos, N., Gavaises, M., Numerical investigation of heavy fuel droplet-particle collisions in the injection zone of a Fluid Catalytic Cracking reactor, part II: 3D simulations, *Fuel Processing Technology*, 156, 2017, 43–53.

[12] Milacic, E., Baltussen, M.W., Kuipers, J.A.M., Direct numerical simulation study of droplet spreading on spherical particles, *Powder Technology*, 354, 2019, 11–18.

[13] Gac, J.M., Gradoń, L., Lattice-Boltzmann modeling of collisions between droplets and particles, *Colloids and Surfaces A: Physicochemical and Engineering Aspects*, 441, 2014, 831–836.

[14] Yang, B., Chen, S., Simulation of interaction between a freely moving solid particle and a freely moving liquid droplet by lattice Boltzmann method, *International Journal of Heat and Mass Transfer*, 127, 2018, 474–484.

[15] Prieto, J.L., Stochastic particle level set simulations of buoyancy-driven droplets in non-Newtonian fluids, *Journal of Non-Newtonian Fluid Mechanics*, 226, 2015, 16–31.

[16] Kaiser, J.W.J., Appel, D., Fritz, F., Adami, S., Adams, N.A., A multiresolution local-timestepping scheme for particle–laden multiphase flow simulations using a level-set and point-particle approach, *Computer Methods in Applied Mechanics and Engineering*, 384, 2021, 113966.

[17] Kwon, T.J., Heistery, S.D., Modeling droplet impact on dry and wet walls, *38th AIAA/ASME/SAE/ASEE Joint Propulsion Conference and Exhibit*, Indianapolis, Indiana, AIAA 2002-4178, 2002.

[18] França, H.L., Oishi, C.M., Thompson, R.L., Numerical investigation of shear-thinning and viscoelastic binary droplet collision, *Journal of Non-Newtonian Fluid Mechanics*, 302, 2022, 104750.

[19] Liu, D., Zhang, P., Law, C.K., Guo, Y., Collision dynamics and mixing of unequal-size droplets, *International Journal of Heat and Mass Transfer*, 57, 2013, 421–428.

[20] Tanguy, S., Ménard, T., Berlemont, A., Estivalezes, J.L., Couderc, F., Méthode réglée de niveau pour le cheminement d'interface : développement et applications, *La Houille Blanche*, 92(2), 2006, 23–31.

[21] Tkachenko, P.P., Shlegel, N.E., Strizhak, P.A., Experimental research of liquid droplets colliding with solid particles in a gaseous medium, *Chemical Engineering Research and Design*, 177, 2022, 200–209.

[22] Charalampous, G., Hardalupas, Y., Collisions of droplets on spherical particles, *Physics of Fluids*, 29, 2017, 103305.

[23] Banitabaei, S.A., Amirfazli, A., Droplet impact onto a solid sphere in mid-air: Effect of viscosity, gas density, and diameter ratio on impact outcomes, *Physics of Fluids*, 32, 2020, 037102.

[24] Sechenyh, V., Amirfazli, A., An experimental study for impact of a drop onto a particle in mid-air: The influence of particle wettability, *Journal of Fluids and Structures*, 66, 2016, 282–292.

[25] Pawar, S.K., Henrikson, F., Finotello, G., Padding, J.T., Deen, N.G., Jongsma, A., Innings, F., Kuipers, J.A.M.H., An experimental study of droplet-particle collisions, *Powder Technology*, 300, 2016, 157–163.

[26] Huang, K.-L., Pan, K.-L., Transitions of bouncing and coalescence in binary droplet collisions, *Journal of Fluid Mechanics*, 928, 2021, A7.

[27] Al-Dirawi, K.H., Al-Ghaithi, K.H.A., Sykes, T.C., Castrejón-Pita, J.R., Bayly, A.E., Inertial stretching separation in binary droplet collisions, *Journal of Fluid Mechanics*, 927, 2021, A9.

[28] Lain, S., Sommerfeld, M., Influence of droplet collision modelling in Euler/Lagrange calculations of spray evolution, *International Journal of Multiphase Flow*, 132, 2020, 103392.

[29] Banitabaei, S.A., Amirfazli, A., Droplet impact onto a solid sphere: Effect of wettability and impact velocity, *Physics of Fluids*, 29, 2017, 062111.

[30] Stow C.D., Hadfield M.G., An experimental investigation of fluid flow resulting from the impact of a water drop with an unyielding dry surface, *Proceedings of the Royal Society of London. A. Mathematical and Physical Sciences*, 373(1755), 1981, 419–441.

[31] Fukai, J., Zhao, Z., Poulikakos, D., Megaridis, C.M., Miyatake, O., Modeling of the deformation of a liquid droplet impinging upon a flat surface, *Physics of Fluids A: Fluid Dynamics*, 5(11), 1993, 2588–2599.

[32] Šikalo, Š., Marengo, M., Tropea, C., Ganić, E., Analysis of impact of droplets on horizontal surfaces, *Experimental Thermal and Fluid Science*, 25, 2002, 503–510.

[33] Roisman, I. V., Berberović, E., Tropea, C., Inertia dominated drop collisions. I. On the universal flow in the lamella, *Physics of Fluids*, 21, 2009, 052103.

[34] Philippi, J., Lagrée, P.-Y., Antkowiak, A., Drop impact on a solid surface: short-time self-similarity, *Journal of Fluid Mechanics*, 795, 2016, 96–135.

[35] Pournaderi, P., Deilami, M., Modeling nanofluid droplet impingement on a superheated surface, *Powder Technology*, 381, 2021, 68–81.

[36] Rozhkov, A., Prunet-Foch, B., Vignes-Adler, M., Impact of drops of polymer solutions on small targets, *Physics of Fluids*, 15, 2003, 2006–2019.

[37] Juarez, G., Gastopoulos, T., Zhang, Y., Siegel, M.L., Arratia, P.E., Splash control of drop impacts with geometric targets, *Physical Review E*, 85(2), 2012, 026319.

[38] Rozhkov, A., Prunet-Foch, B., Vignes-Adler, M., Impact of water drops on small targets, *Physics of Fluids*, 14, 2002, 3485–3501.

[39] Hung, L.S., Yao, S.C., Experimental investigation of the impaction of water droplets on cylindrical objects, *International Journal of Multiphase Flow*, 25, 1999, 1545–1559.

[40] Chung, C., Lee, M., Char, K., Ahn, K.H., Lee, S.J., Droplet dynamics passing through obstructions in confined microchannel flow, *Microfluidics and Nanofluidics*, 9, 2010, 1151–1163.

[41] Zhang, D., Papadikis, K., Gu, S., Investigations on the Droplet Impact onto a Spherical Surface with a High Density Ratio Multi-Relaxation Time Lattice-Boltzmann Model, *Communications in Computational Physics*, 16(4), 2014, 892–912.

[42] Liang, G., Guo, Y., Yang, Y., Shen, S., Liquid sheet behaviors during a drop impact on wetted cylindrical surfaces, *International Communications in Heat and Mass Transfer*, 54, 2014, 67–74.

[43] Hardalupas, Y., Taylor, A.M.K.P., Wilkins, J.H., Experimental investigation of sub-millimetre droplet impingement onto spherical surfaces, *International Journal of Heat and Fluid Flow*, 20, 1999, 477–485.

[44] Bakshi, S., Roisman, I. V., Tropea, C., Investigations on the impact of a drop onto a small spherical target, *Physics of Fluids*, 19, 2007, 032102.

[45] Ge, Y., Fan, L.S., Droplet - Particle collision mechanics with film-boiling evaporation, *Journal of Fluid Mechanics*, 573, 2007, 311–337.

[46] Yan-Peng, L., Huan-Ran, W., Three-dimensional direct simulation of a droplet impacting onto a solid sphere with low-impact energy, *The Canadian Journal of Chemical Engineering*, 89(1), 2011, 83–91.

[47] Mitra, S., Sathe, M.J., Doroodchi, E., Utikar, R., Shah, M.K., Pareek, V., Joshi, J.B., Evans, G.M., Droplet impact dynamics on a spherical particle, *Chemical Engineering Science*, 100, 2013, 105–119.

[48] Zhang, D., Papadikis, K., Gu, S., Application of a high density ratio lattice-Boltzmann model for the droplet impingement on flat and spherical surfaces, *International Journal of Thermal Sciences*, 84, 2014, 75–85.

[49] Dubrovsky, V. V., Podvysotsky, A.M., Shraiber, A.A., Particle interaction in three-phase polydisperse flows, *International Journal of Multiphase Flow*, 18, 1992, 337–352.

[50] Mitra, S, Evans, G.M., Doroodchi, E., Pareek, V., Joshi, J.B., Interactions in droplet and particle system of near unity size ratio, *Chemical Engineering Science*, 170, 2017, 154–175.

[51] Mitra, S., Doroodchi, E., Pareek, V., Joshi, J.B., Evans, G.M., Collision behaviour of a smaller particle into a larger stationary droplet, *Advanced Powder Technology*, 26(1), 2015, 280–295.

[52] Yoon, I., Shin, S., Maximal spreading of droplet during collision on particle: Effects of liquid viscosity and surface curvature, *Physics of Fluids*, 33, 2021, 083310.

[53] Wu, G., Chen, S., Simulating the collision of a moving droplet against a moving particle: Impact of Bond number, wettability, size ratio, and eccentricity, *Physics of Fluids*, 33, 2021, 093313.

[54] Pasternak, L., Mañas, J.M., Sommerfeld, M., Influence of droplet properties on the coating of free-falling spherical particles, *Atomization and Sprays*, 31(2), 2021, 37–61.

[55] Gumulya, M., Utikar, R.P., Pareek, V., Mead-Hunter, R., Mitra, S., Evans, G.M., Evaporation of a droplet on a heated spherical particle, *Chemical Engineering Journal*, 278, 2015, 309–319.

[56] Wu, G., Chen, S., Du, W., Zhai, S., Zeng, S., Yu, Y., Zhou, W., Simulation on a three-dimensional collision of a moving droplet against a moving super-hydrophobic particle, *Powder Technology*, 405, 2022, 117558.

[57] Munnannur, A., Reitz, R.D., A new predictive model for fragmenting and non-fragmenting binary droplet collisions, *International Journal of Multiphase Flow*, 33, 2007, 873–896.

[58] Shlegel, N.E., Tkachenko, P.P., Strizhak, P.A., Collision of water droplets with different initial temperatures, *Powder Technology*, 367, 2020, 820–830.

[59] Rabe, C., Malet, J., Feuillebois, F., Experimental investigation of water droplet binary collisions and description of outcomes with a symmetric Weber number, *Physics of Fluids*, 22, 2010, 47101.

[60] Mitra, S., Nguyen, T.B.T., Doroodchi, E., Pareek, V., Joshi, J.B., Evans, G.M., On wetting characteristics of droplet on a spherical particle in film boiling regime, *Chemical Engineering Science*, 149, 2016, 181–203.

[61] Mitra, S., Evans, G., Dynamic surface wetting and heat transfer in a droplet-particle system of less than unity size ratio, *Frontiers in Chemistry*, 6, 2018, 1–19.

[62] Malgarinos, I., Nikolopoulos, N., Marengo, M., Antonini, C., Gavaises, M., VOF simulations of the contact angle dynamics during the drop spreading: Standard models and a new wetting force model, *Advances in Colloid and Interface Science*, 212, 2014, 1–20.

[63] Hirt, C., Nichols, B., Volume of fluid (VOF) method for the dynamics of free boundaries, *Journal of Computational Physics*, 39(1), 1981, 201–225.

[64] Brackbill, J., Kothe, D., Zemach, C., A continuum method for modeling surface tension, *Journal of Computational Physics*, 100(2), 1992, 335–354.

[65] Ubbink, O., *Numerical prediction of two fluid systems with sharp interfaces*, Ph.D. Thesis, Department of Mechanical Engineering, Imperial College of Science, Technology & Medicine, London, UK, 1997.

[66] Shlegel, N.E., Strizhak, P.A., Volkov, R.S., Collision Behavior of Heterogeneous Liquid Droplets, *Microgravity Science and Technology*, 31, 2019, 487–503.

[67] Islamova, A.G., Kerimbekova, S.A., Shlegel, N.E., Strizhak, P.A., Droplet-droplet, droplet-particle, and droplet-substrate collision behavior, *Powder Technology*, 403, 2022, 117371.

[68] Antonov, D.V., Shlegel, N.E., Strizhak, P.A., Tarlet, D., Bellettre, J., Energy analysis of secondary droplet atomization schemes, *International Communications in Heat and Mass Transfer*, 117, 2020, 104666.

[69] Karl, A., Anders, K., Rieber, M., Frohn, A., Deformation of liquid droplets during collisions with hot walls: Experimental and Numerical Results, *Particle & Particle Systems Characterization*, 13(3), 1996, 186–191.

[70] Shlegel, N.E., Tkachenko, P.P., Strizhak, P.A., Influence of viscosity, surface and interfacial tensions on the liquid droplet collisions, *Chemical Engineering Science*, 220, 2020, 115639.

[71] Vilela, V., de Souza, F.J., A Numerical Study on Droplet-Particle Collision, *Flow, Turbulence and Combustion*, 105, 2020, 965–987.

[72] Rioboo, R., Tropea, C., Marengo, M., Outcomes from a Drop Impact on Solid Surfaces, *Atomization and Sprays*, 11(2), 2001, 12.

[73] Zhang, Y., Xu, Z., Tu, Y., Wang, J., Li, J., Study on properties of coal-sludge-slurry prepared by sludge from coal chemical industry, *Powder Technology*, 366, 2020, 552–559.

[74] Antonov, D. V., Valiullin, T.R., Iegorov, R.I., Strizhak, P.A., Effect of macroscopic porosity onto the ignition of the waste-derived fuel droplets, *Energy*, 119, 2017, 1152–1158.

[75] Piskunov, M.V., Shlegel, N.E., Strizhak, P.A., Disruption of colliding liquid droplets with different surface geometries, *Powder Technology*, 355, 2019, 526–534.

[76] Webber, G.B., Manica, R., Edwards, S.A., Carnie, S.L., Stevens, G.W., Grieser, F., Dagastine, R.R., Chan, Dynamic Forces between a Moving Particle and a Deformable Drop, *The Journal of Physical Chemistry C*, 112(2), 2008, 567–574.

[77] Voitkov, I.S., Volkov, R.S., Strizhak, P.A., Temperature of gases in a trace of water droplets during their motion in a flame, *Thermal Science*, 22, 2018, 335–346.

[78] Tonini, S., Gavaises, M., Theodorakakos, A., The role of droplet fragmentation in high-pressure evaporating diesel sprays, *International Journal of Thermal Sciences*, 48, 2009, 554–572.

[79] Tonini, S., Cossali, G.E., An analytical model of liquid drop evaporation in gaseous environment, *International Journal of Thermal Sciences*, 57, 2012, 45–53.

ORCID iD

Dmitrii V. Antonov https://orcid.org/0000-0002-2763-2708
Roman M. Fedorenko https://orcid.org/0000-0003-1048-4742
Pavel A. Strizhak https://orcid.org/0000-0003-1707-5335

Publisher's Note Shahid Chamran University of Ahvaz remains neutral with regard to jurisdictional claims in published maps and institutional affiliations.